Human Molecular Genetics, 2023, Vol. 32, 7, 1184–1192
https://doi.org/10.1093/hmg/ddac257
Advance access publication date 10 November 2022
Original Article

Syntaxin 4 is essential for hearing in human and zebrafish

Isabelle Schrauwen[1,†], Amama Ghaffar[2,†], Thashi Bharadwaj[1], Khadim Shah[3], Sakina Rehman[2], Anushree Acharya[1], Khurram Liaqat[1], Nicole S. Lin[1], Jenna L. Everard[1], Anwar Khan[4], Zubair M. Ahmed[2], Wasim Ahmad[5], Saima Riazuddin[2] and Suzanne M. Leal[1,6,*]

[1]Center for Statistical Genetics, Sergievsky Center, and the Department of Neurology, Columbia University Medical Center, New York, NY, USA
[2]Department of Otorhinolaryngology - Head & Neck Surgery, School of Medicine University of Maryland, Baltimore, MD, USA
[3]Department of Biotechnology, COMSATS University Islamabad, Abbottabad Campus, Khyber Pakhtunkhwa, Pakistan
[4]Department of Biochemistry, Hazara University Mansehra, Khyber Pakhtunkhwa, Pakistan
[5]Department of Biochemistry, Faculty of Biological Sciences, Quaid-i-Azam University Islamabad, Islamabad, Pakistan
[6]Taub Institute for Alzheimer's Disease and the Aging Brain, and the Department of Neurology, Columbia University Medical Center, New York, NY, USA
*To whom correspondence should be addressed at: Center for Statistical Genetics, Sergievsky Center, Taub Institute for Alzheimer's Disease and the Aging Brain and the Department of Neurology, Columbia University, 630 W 168th St, New York, NY 10032, USA. Tel: +1 (212) 304-7047; Email: sml3@cumc.columbia.edu
†These authors contributed equally.

Abstract

Congenital hearing impairment (HI) is a genetically highly heterogeneous disorder in which prompt recognition and intervention are crucial to optimize outcomes. In this study, we used exome sequencing to investigate a large consanguineous Pakistani family with eight affected individuals showing bilateral severe-to-profound HI. This identified a homozygous splice region variant in *STX4* (c.232 + 6T>C), which causes exon skipping and a frameshift, that segregated with HI (two-point logarithm of odds (LOD) score = 5.9). STX4, a member of the syntaxin family, is a component of the SNARE machinery involved in several vesicle transport and recycling pathways. *In silico* analysis showed that murine orthologue *Stx4a* is highly and widespread expressed in the developing and adult inner ear. Immunofluorescent imaging revealed localization of STX4A in the cell body, cell membrane and stereocilia of inner and outer hair cells. Furthermore, a morpholino-based knockdown of *stx4* in zebrafish showed an abnormal startle response, morphological and developmental defects, and a disrupted mechanotransduction function in neuromast hair cells measured via FM1–43 uptake. Our findings indicate that STX4 dysfunction leads to HI in humans and zebrafish and supports the evolutionary conserved role of STX4 in inner ear development and hair cell functioning.

Introduction

Hearing impairment (HI) affects between 1 and 2 newborns per 1000 and impacts speech development, education and overall quality of life, resulting in a significant financial burden on families and healthcare systems. As such, early detection and accurate diagnosis are imperative to optimize intervention and improve outcomes. Approximately 50%–60% of congenital HI has a genetic etiology (1,2). The complexity of the human hearing system is reflected by its highly diverse genetic etiology, with over 120 genes identified for non-syndromic (NS) HI alone (3). Current genetic testing for HI is mainly driven by gene panels, with some adoption of exome sequencing (4–7). Nevertheless, its diagnostic rates are based on existing knowledge of the genetic etiology of HI, resulting in current diagnostic rates ranging from 28% to 52% (4–7). The discovery of novel genes and variants implicated in HI is therefore crucial to improve diagnostic rates and allow more personalized interventions.

The syntaxins (STXs) are a family of proteins involved in vesicle fusion in diverse vesicular transport processes along the exocytic and the endocytic pathway (8). They are part of a larger structural group of proteins that mediate membrane vesicle fusion called soluble *N*-ethyl malemide sensitive factor adaptor protein receptors (SNAREs), which are highly conserved amongst all eukaryotes (9). The inner ear sensory hair cells, responsible for translating sound induced mechanical vibrations in the cochlea into electric signals and neurotransmission (i.e. mechanotransduction), contain two specialized areas of membrane delivery: one located at the apex and one at the cell base (10). The first area at the apex of the hair cells, around the cuticular plate that anchors the stereocilia, accommodates the continuous mechanical movement of stereocilia and facilitates their repair via the recycling of membrane components (10). The second area is the afferent synapse at the hair cell base, where neurotransmitter release is mediated via a Ca^{2+} influx and subsequent synaptic vesicle exocytosis and recycling (10,11). SNARE proteins, including syntaxin 1, are concentrated at both sides of hair cells and at both of these locations are involved in vesicle fusion (10).

In this study, we describe a novel cause of human HI due to defects in syntaxin 4 that was identified through the study of a large consanguineous Pakistani family segregating NSHI with an autosomal recessive (AR) mode of inheritance. STX4 is one of the members of the syntaxin family and previously shown to be involved in several vesicle transport pathways (8).

Received: April 19, 2022. **Revised:** August 22, 2022. **Accepted:** November 11, 2022

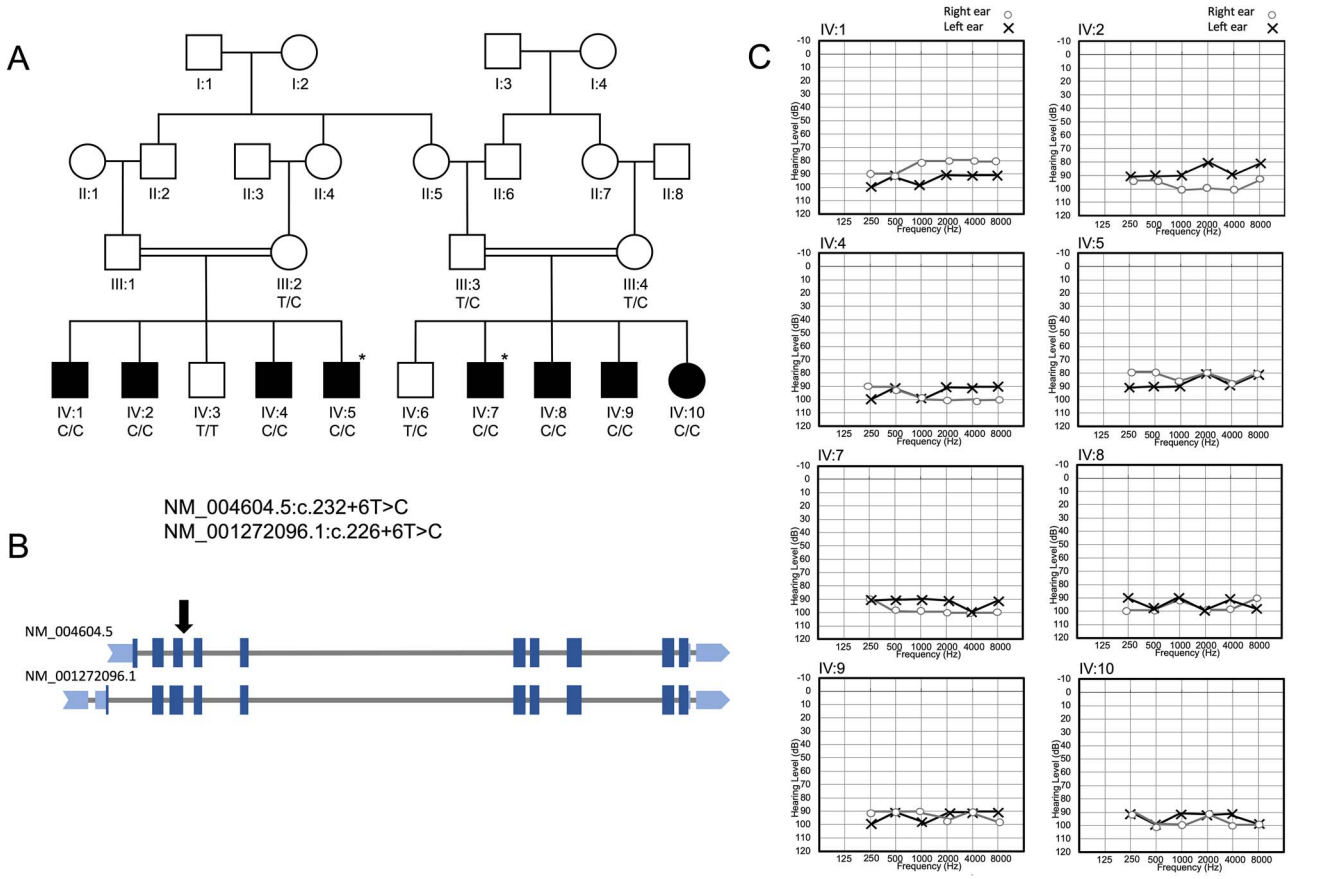

Figure 1. Genetic and audiometric data for Pakistani family members with HI due to a splice region variant in *STX4*. (**A**) Family 4768 pedigree drawing displaying the segregation of the c.232 + 6T>C *STX4* variant. Hearing impaired family members are indicated by a black box (male) or circle (female). Individuals who had a DNA sample that underwent exome sequencing are indicated with an asterisk. (**B**) STX4 coding isoforms according to GENCODEv39 and location of the splice region variant (indicated with an arrow). (**C**) Pure-tone audiometry audiograms for hearing impaired family members; x represents the results for the left ear and o for the right ear. Affected individuals show severe-to-profound or profound HI. Ages at which the audiometry was performed: IV:1 [25 years of age], IV:2 (22 year), IV:4 (20 year), IV:5 (21 year), IV:7 (10 year), IV:8 (12 year), IV:9 (14 year) and IV:10 (15 year).

Results

Clinical findings

Pure tone audiometry showed a bilateral severe-to-profound or profound HI in affected individuals (Fig. 1), and no HI in the parents (Supplementary Material, Fig. S1). No vestibular dysfunction was found in hearing-impaired family members. Facial features were normal, and no neurological abnormality was observed in the affected individuals. An electrocardiogram was recorded in two affected family members (IV:7 and IV:8), which did not show any abnormalities. Head circumference was increased but within normal limits in affected individuals tested (IV:1, IV:5, IV:7, IV:8, IV:9, IV:10), except for one individual (IV:1) who showed borderline macrocephaly (+2.0 SD) (Supplementary Material, Table S1).

Exome sequencing

Exome sequencing revealed candidate variants in several genes (*PIGV, COL6A6, DUOX2, MYO15A, KCNJ10, WDFY3* and *STX4*; Supplementary Material, Table S2). Sanger sequencing was performed to test segregation in the remaining family members, after which only one variant was found to segregate with HI in the family (Fig. 1). This was a splice region variant in *STX4* (NM_001272096.1:c.226 + 6T>C;NM_004604.5:c.232 + 6T>C), predicted to impact splicing by computational tools, including dbscSNV1.1 (dbscSNV$_{ADA}$: 0.99; dbscSNV$_{RF}$: 0.90) (12), NNSPLICE0.9 (wild-type [WT] 5′ donor loss) (13) and Human Splicing Finder Professional (Broken WT Donor site; −42.66%) (14). The variant has a Combined Annotation Dependent Depletion (CADD) score of 23 and is present with a low frequency in the Genome Aggregation Database (gnomAD)v2 database (MAF = 7.98×10^{-6}), where it is found in the heterozygous state in two individuals of non-Finnish European descent. It is absent from the Trans-Omics for Precision Medicine (TOPMed) Bravo database (15), gnomADv3 (16), The Greater Middle East (GME) (17) and the All of Us research program data (11/29/2021 release) (18). Last, no copy number variants (CNV)s in known HI genes or in any other clinically relevant regions were found.

There are two protein coding isoforms for *STX4* in GENCODEv39 and Uniprot predicts alternative splicing (NM_004604.5/ENST00000313843.8 and NM_001272096.1/ENST00000394998.5; Fig. 1). In the Genotype-Tissue Expression (GTEx) atlas, the canonical isoform NM_004604.5 has the most prominent expression across all tissues (19); this is also the case in the human inner ear (20). It is predicted to lead to a loss of the 5′ donor by the computational tools mentioned above, which can lead to exon skipping of coding exon 3, which we verified as described in the mini-gene assay. This will result in a frameshift for both human transcript isoforms, predicted to be targeted by nonsense mediated decay (21).

Homozygosity mapping and linkage analysis

Homozygosity mapping revealed only two regions of shared homozygosity for the affected individuals IV:5 and IV:7, on chr3p21.1 (596kbp) and chr16p12.1-q12.2 (30.7 Mb). The *STX4* variants resided in the homozygous chr16 region, and two-point linkage analysis of the *STX4* homozygous variants revealed a logarithm of odds (LOD) score of 5.9 at theta = 0.0.

Minigene splicing assay of the *STX4* c.232 + 6T>C variant

The PCR product amplified from the cDNA of both control ($STX4^{WT}$) and mutant ($STX4^{c.232+6T>C}$) containing exons 2–4 of human *STX4* showed a size difference consistent with the skipping of exon 3 (Supplementary Material, Fig. S2). Exon skipping of exon 3 was further confirmed through Sanger sequencing (Supplementary Material, Fig. S2C).

Stx4a mRNA and protein expression in the mouse inner ear

The murine orthologue of human *STX4* is *Stx4a*, which encodes for murine protein STX4A. *In silico* analysis of mice RNA expression datasets show that murine orthologue *Stx4a* is highly expressed during inner ear development (Supplementary Material, Figs S3–S11). Expression in the sensory epithelium is widespread (Supplementary Material, Figs S3, S5–11) and *Stx4a* is upregulated during later developmental stages, including the inner and outer hair cells (Supplementary Material, Figs S3, S8–S11). Expression is also found in the spiral and vestibular ganglion cells, and here also upregulated at later developmental stages (Supplementary Material, Fig. S3). *Stx4a* is also expressed widely during early craniofacial development, such as in the paraxial mesoderm (E8.5) and maxillary arch epidermal ectoderm (E9.5) (Supplementary Material, Fig. S4). We next performed whole mount immunostaining of STX4A in cochlear tissue of P12 WT mice. This revealed STX4A immunoreactivity at stereocilia level as well as throughout the outer and inner hair cells bodies and in the plasma membrane (Fig. 2 and Supplementary Material, Fig. S12).

Morpholino-based knockdown of *stx4* in zebrafish

We performed a morpholino-based knockdown of *stx4* in zebrafish targeting the ATG start codon site and the corresponding zebrafish 5′ donor splice site (SS) as affected by the c.232 + 6T>C variant in the human *STX4* orthologue. However, reverse transcription - polymerase chain reaction (RT-PCR) confirmed intron 3 retention between exon 3 and exon 4 due to the SS covering *stx4* morpholino (Fig. 3C). At 5 days post fertilization (dpf), acoustic evoked behavioral response (ABER) assessment was done on 9ng ATG and SS morpholino injected zebrafish larvae in comparison to 9ng injected control. It was observed that both ATG and SS morphants showed a significant difference in response to stimuli as compared to controls; $P = 0.0001$ and 0.0017, respectively (Fig. 3B). Moreover, the *stx4* morpholinos (ATG and SS) injected zebrafish larvae showed severe morphological developmental defects with edema (Fig. 3D). We further measured the head to length ratios for 9ng injected control versus 9ng injected ATG morphs and SS morphs respectively and observed a significant difference of $P = 0.0001$ for both comparisons. Both *stx4*-injected larva types had a greater head size as compared to control injected larvae (Fig. 3E). Next, to assess the mechano-transduction function of neuromast cells after injecting 9ng *stx4* morpholino, zebrafish larvae at 5 dpf were processed for FM1–43 dye uptake. Neuromast cells of 9ng *stx4* morpholinos (ATG and SS) injected zebrafish larvae did not uptake any FM1–43 dye (Fig. 3F) suggesting that these cells have a disrupted mechanotransduction function as compared to the neuromast cells of 9ng control injected control larvae, which took up the FM1–43 dye (Fig. 3F). These findings demonstrate that morpholino-based knockdown of *stx4* in zebrafish leads to loss of hearing and mechanotransduction function along with some severe morphological defects.

Discussion

STX4 is known to function in the SNARE machinery and involved in different forms of regulated vesicle transport in diverse cell types (22–26). In rat hippocampal neurons, STX4 acts as a postsynaptic t-SNARE important in postsynaptic plasticity including rapid modification of dendritic spines during the many membrane trafficking events such as the fusion of recycling endosomes (24). In addition, STX4 is involved in glucose-triggered insulin secretion in pancreatic β cells, IgE-dependent granule release from mast cells, and insulin-regulated glucose transporter (GLUT4) translocation from intracellular vesicles to the plasma membrane in adipocytes and myocytes (22,24,25,27–33). Its function in the auditory system however has not been studied. A recent study shows that *Stx4* mRNA is upregulated in response to trauma caused by acoustic overstimulation in rat cochlea (34). In this study, we show that syntaxin 4 is crucial for sound perception in both humans and zebrafish.

We studied a large consanguineous Pakistani family with AR HI that segregates a *STX4* splice region variant (NM_004604.5:c.232 + 6T>C) with a significant two-point LOD score of 5.9 at theta = 0. The variant is very rare in population databases and is predicted to lead to a loss of the 5′ donor at the WT SS position of all coding isoforms. The variant was confirmed to cause exon skipping in a minigene assay, which leads to a frameshift targeted by nonsense-mediated decay. STX4 is highly expressed throughout the body (19), including the brain where it is localized mainly in the hippocampus and neocortex (24). We show it is also widely expressed in the developing and adult inner ear, including the sensory epithelium, hair cells, spiral and vestibular ganglion cells, and upregulated during development. Via immunohistochemistry we show that it is expressed in both inner and outer hair cells of P12 mice, both in the stereocilia, cytoplasm and cell membrane.

To confirm its function in hearing and in the sensory epithelium, we next performed a knockdown of *stx4* in zebrafish via morpholinos targeting the ATG start codon site and the SS donor corresponding with the human c.232 + 6T>C variant at the exon 3–intron 3 boundary. The SS blocker led to the in-frame retention of intron 3 and creation of premature stop codon via the novel inserted sequence in the mRNA. ABER-based startle response at 5 days post fertilization (dpf) showed a significant reduction of startle response to 1kHz frequency stimuli for both types of *stx4*-injected morphants (ATG and SS) as compared to 9ng control injected larvae, suggesting impaired hearing in *stx4*-injected morphants. In addition, *stx4*-injected larvae also showed increased head sizes consistent with the increased head size measurements in the hearing impaired family members; however, the measurements in the affected family members did not reach the criteria of macrocephaly with exception of one affected who was borderline macrocephalic. Last, the human variant c.232 + 6T>C showed exon 3 skipping, not intron retention as in the zebrafish, which both may reflect a difference in local splicing regulation in both

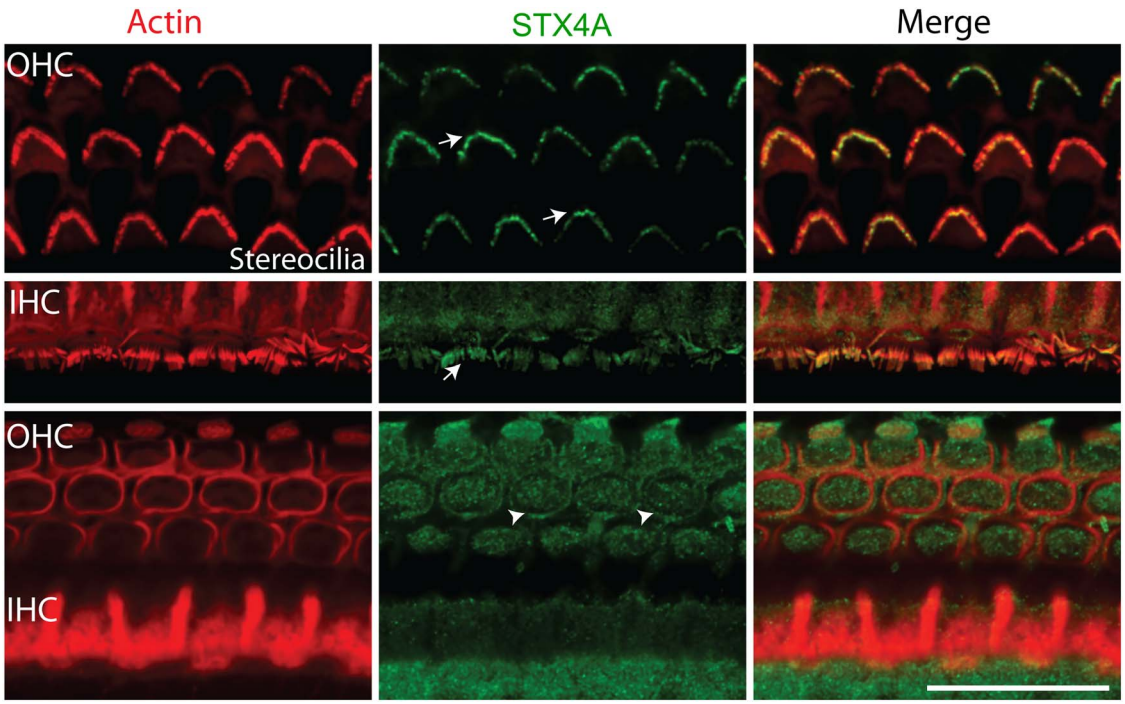

Figure 2. STX4A is expressed in the outer and inner hair cells of the mouse cochlea. Whole mount cochlear tissue from P12 wild-type mice were immunolabeled with anti-syntaxin 4 antibody (green), while phalloidin (red) was used to decorate F-actin cytoskeleton. STX4A (green) was localized in the stereocilia (arrows) of both outer and inner hair cells. Also, STX4A expression was observed in hair cells' body and cell membrane (arrowheads). Scale bar, 20μm.

species. Nonetheless, the predicted loss of function of STX4/Stx4 in both results into a similar phenotype.

Hair cells contain mechanosensitive channels that quickly open in response to sound-induced vibrations. To assess mechanosensitive channel function in the hair cells in the neuromasts of the lateral line, we briefly exposed injected and non-injected larvae to FM1–43, a styryl pyridinium dye that penetrates hair cells first via mechanotransduction channels at the tips of the stereocilia (35). There was apparently no FM1–43 dye uptake in neuromast hair cells of *stx4*-injected larvae, suggesting a disrupted mechanotransduction in the hair cells of the neuromast. As mentioned previously, STXs are implicated in vesicle transport and recycling at the two trafficking hotspots in hair cells (at the apex and base). Intense vesicle transport at the apex of hair cells occurs in a narrow region between the cuticular plate and the junctional complexes (10, 36), and supports the functioning and repair of stereocilia which perform a continuous mechanical movement in response to sound (10). Aberrant STX4 might impact the mechanotransduction complex organization and function via hindering the normal vesicle trafficking in hair cells.

As syntaxins are also important in synaptic signaling and exocytosis in neurons (24), STX4 dysfunction may also affect afferent synaptic transmission from hair cells to downstream nerves (37). Otoferlin (*OTOF*), for example, interacts with both syntaxin 1 and SNAP25 at the afferent ribbon synapses in inner hair cells of the cochlea to trigger exocytosis and release of the neurotransmitter glutamate (38). Defects in this process due to *OTOF* dysfunction cause AR hearing loss in both mouse and man (38). Further studies in animal models (e.g. mouse model) would help in deciphering the precise role of STX4 in the cochlear hair cells and synaptic machinery development and function.

A recent study also implicated *stx4* in cardiac development in zebrafish, with myocardial dysfunction, bradycardia and aberrations in Ca^{2+} handling noted in CRISPR-Cas9 *stx4* mutant zebrafish larvae (39). Furthermore, otic vesicle dysgenesis was noted amongst the multiple defects. The authors also identified biallelic *STX4* variants in two patients with a severe multisystem disease including cardiac dysfunction. Although the association of *STX4* with this human multisystem disease needs further confirmation, one of the two patients with a homozygous p.R240W *STX4* variant also displayed sensorineural hearing loss (39).

Last, we screened for *STX4* variants in our in-house exome dataset of 473 families with hearing loss, of which of which 441 are Pakistani families and primarily consanguineous. Although a second family could not be identified and is likely a rare cause of hearing loss, we recommend adding this gene to diagnostic hearing loss panels to propel the identification of novel families. Last, the identification of additional families will also clarify if macrocephaly is an additional feature associated with *STX4* hearing loss disorder.

In conclusion, we identified a novel key player, STX4, crucial in hearing and mechanotransduction in the inner ear sensory epithelium in humans and zebrafish. This finding expands the genetic etiology underlying HI and will improve genetic diagnostic testing.

Materials and Methods

Sample collection and clinical evaluation

The study was approved by the Institutional review board of Columbia University (IRB-AAAS2343) and the ethics committee of the Quaid-i-Azam University (IRB-QAU-153). Written informed consent was obtained from all participating members of a large consanguineous family from the Khyber Pakhtunkhwa province in Pakistan (Family 4768; Fig. 1). Peripheral blood samples were collected and DNA was extracted using a phenol chloroform

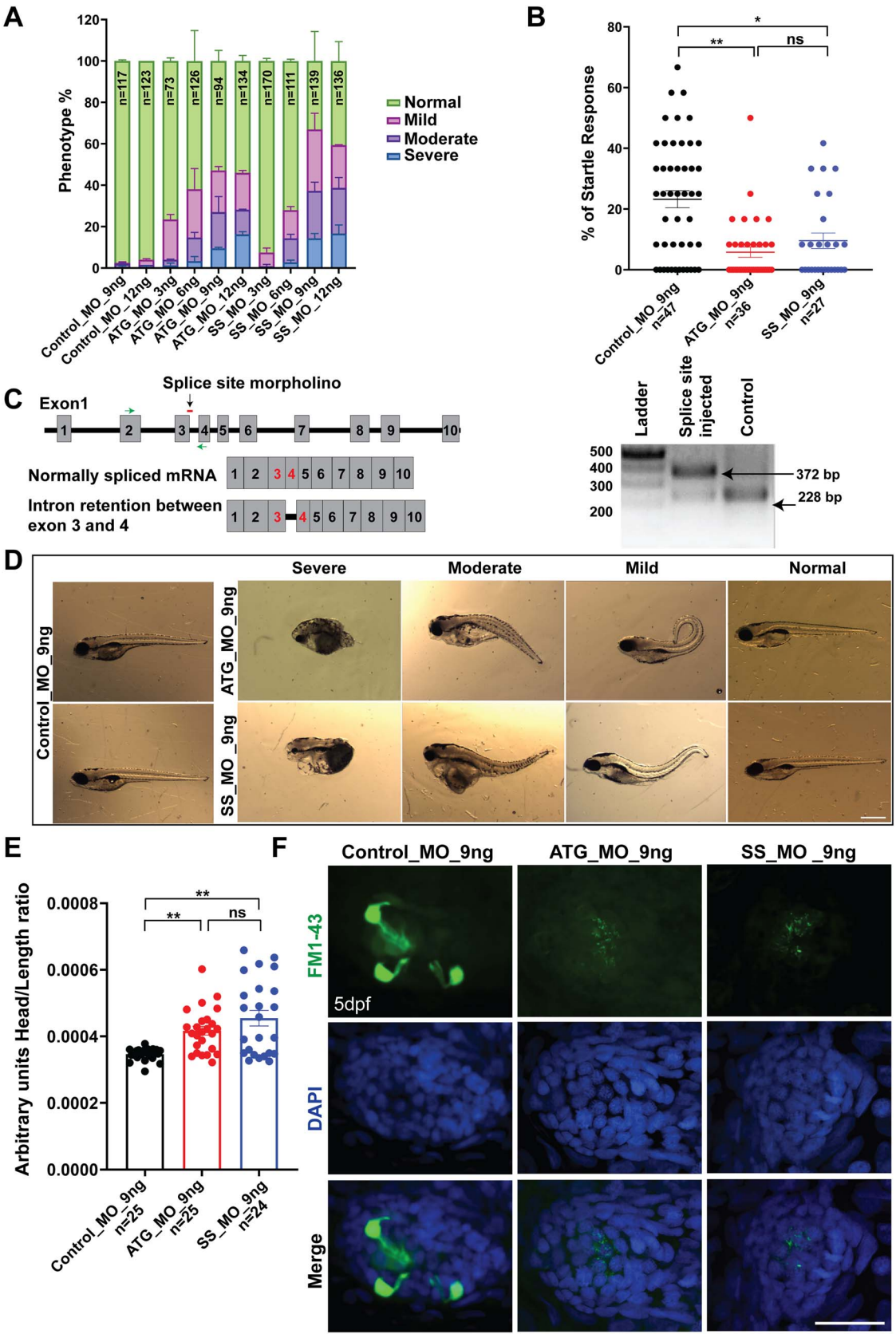

Figure 3. Morpholino-based knockdown of *stx4* in zebrafish causes deficits of hearing and mechanotransduction. (**A**) Phenotype assessment based on dosage response for both ATG and SS blockers for *stx4*. Class severe: defect in eye formation, no tail, small body size and edema; Class moderate: edema and curved body, class mild: curved body and class normal: no visible deformities. (**B**) ABER in 9ng control injected versus 9ng injected ATG blocker (**$P = 0.0001$) and 9ng control injected versus 9ng SS injected morphs (*$P = 0.0017$) showing a significant difference. Approximately 9ng ATG vs 9ng SS morphants did not show a significant difference ($P = 0.2031$). (**C**) Schematic representation of the zebrafish *stx4* gene showing the position of SS morpholino (red line) at the end of exon 3 and start of intron 3. Green line arrows indicate primers used for amplification. The bar diagram shows

protocol (40). DNA samples were obtained from eight affected and five unaffected family members, respectively (Fig. 1; III:2–4; IV:1–10). A clinical history was obtained from family members, and a physical and neurological examination was also performed. To evaluate hearing and vestibular functioning, pure-tone audiometry (250–8000 Hz), and tandem gait and Romberg tests were performed in all affected individuals [IV:1 [25 year of age], IV:2 (22 year), IV:4 (20 year), IV:5 (21 year), IV:7 (10 year), IV:8 (12 year), IV:9 (14 year) and IV:10 (15 year)]. Pure-tone audiometry was also recorded in carrier parents: III:2 (52 year), III:3 (48 year), III:4 (43 year). Other underlying causes of HI, including infections, ototoxic medications and trauma, were excluded. In addition, for two affected individuals (IV:7 and IV:8) an electrocardiogram was recorded.

Exome sequencing

Variants in the coding region of *GJB2* and other common genomic variants associated with HI in the Pakistani were excluded prior to exome sequencing via Sanger sequencing [*GJB2* coding region; *CIB2*: p.(Phe91Ser), p.(Cys99Trp); *HGF*: c.482 + 1986_1988delTGA, c.482 + 1991_2000delGATGATGAAA; *SLC26A4*: p.(Gln446Arg), p.(Val239Asp)] (41–43). Next, DNA samples from two hearing impaired family members (IV:5 and IV:7), each from a separate branch of pedigree 4768, underwent exome sequencing (Fig. 1). Exome enrichment was performed using the SureSelect Human All Exon V6 kit (60.46 Mb) and paired-end sequencing was performed on a HiSeq2500/4000 instrument (Illumina Inc, San Diego, CA, USA). An average on target read depth of 94.64x and 112.84x were obtained for the samples from individuals IV:5 and IV:7, respectively. Low-quality reads were removed, and remaining reads were aligned to the human reference genome (GRCh37/Hg19) using Burrows-Wheeler Aligner-MEM (BWAv0.7.15) (44). Duplicate reads were marked using Picard-tools (v2.5.0), and insertions/deletion (InDel)-realignment and base quality score recalibration were performed with the Genome Analysis Toolkit (GATK) (v3.7). Single nucleotide variants (SNVs) and InDels were called by the GATK HaplotypeCaller (45). Variants were annotated using ANNOVAR (46) and custom scripts were used to filter to identify candidate variants. Each branch of the family was also analyzed separately in case of locus heterogeneity, considering an AR mode of inheritance. First, SNVs and InDels with a population specific minor allele frequency (MAF) of < 0.005 in every population of the gnomAD Database (16) and the GME Variome Project (17) were retained. The remaining variants were filtered further by only retaining exonic variants, splice region variants (±12 bp from intron-exon boundary) and variants with a predicted effect on protein function or pre-mRNA splicing (missense, nonsense, frameshift, start-loss, splice region, etc.). Bioinformatic prediction scores were annotated from dbnsfp35a and dbscSNV1.1 to evaluate missense and SS/region variants respectively to aid in selecting variants for further evaluation (12,47), which included, for example, the CADD scores (48). CNVs were called using CONiFER (v0.2.2) (49). Gene annotation was performed using AnnotSV (50) and a custom in-house annotation with BioMart (51), and CNV frequency was assessed using the Database of Genomic Variants (52) and gnomAD (16) using the same frequency cut-offs as above for SNV/InDels. Candidate variants were visualized using the Integrative Genomics Viewer (IGV2.4.3). SNV/Indel variants that were deemed unlikely to be false variant calls based on IGV were validated and checked for segregation in all family members with available DNA samples using Sanger sequencing performed using an ABI3130XL Genetic Analyzer.

Homozygosity mapping and linkage analysis

Homozygous regions shared by affected individuals IV:5 and IV:7 from whom exome data was available were identified after removing multiallelic sites and InDels with BCFtools (53) using Homozygosity mapper (54). Two-point linkage analysis was performed and a LOD score for the segregating variant in *STX4* was computed using Superlink Online 1.1 (55). An AR mode of inheritance with complete penetrance and the gnomAD allele frequency of 7.98×10^{-6} were used for the calculation of the LOD score at theta = 0.

Minigene splicing assay of the *STX4* c.232 + 6T>C variant

The genomic DNA region carrying the exonic and intronic regions from exon 2 to exon 4 of the human *STX4* canonical transcript (NM_004604.5) was amplified and then cloned into a pSPL3 vector carrying splice donor and splice acceptor sites (Supplementary Material, Fig. S2A). The developed clones for both control $STX4^{WT}$ and mutant $STX4^{c.232+6T>C}$ were then sequence verified and used for transfecting Cos7 cells. After 1 day of transfection, cells were collected, and RNA was isolated to develop cDNA. Vector splice donor and splice acceptor site-based primers were used to amplify products and gel electrophoresis was done to indicate a difference between WT and mutant (Supplementary Material, Fig. S2B). The PCR product was then Sanger sequenced to confirm the result (Supplementary Material, Fig. S2C).

In silico mRNA *Stx4a* expression analysis in mouse craniofacial and inner ear tissues

We performed an *in silico* analysis of the expression of mouse orthologue *Stx4a* during mouse development using various publicly available datasets with RNA-seq and/or microarray data of inner ear and craniofacial tissues. First, we studied *Stx4a* expression during early mouse craniofacial development using series GSE55966 from the Gene Expression Omnibus (GEO) database containing RNA sequencing data of CD1 mouse embryos at embryonic day (E)8.5, E9.5, E10.5 (56). Further data manipulation and conversion to TPM (Transcripts Per Kilobase Million) was performed before data visualization. To study *Stx4a* expression during mouse inner ear development, previously generated datasets were obtained from the Shared Harvard Inner-Ear Laboratory Database (SHIELD) (57). The first dataset

a scheme of the normal mRNA produced versus SS morpholino injected zebrafish mRNA retaining with exon 3. RT-PCR gel electrophoresis results showing retention of intron 3 between exon 3 and exon 4 in SS morpholino injected embryos. (**D**) Representative images of 9ng ATG and SS morpholino injected larvae and 9ng control injected larvae at 5 dpf. Severe morphological defects with edema were observed in 9 ng injected larvae as compared to 9ng injected controls. (**E**) Head to length ratio of 9 ng control injected versus 9ng injected ATG blocker and 9ng control injected versus 9ng SS injected morphs showing a significant difference (**$P = 0.0001$). Approximately 9ng ATG versus 9ng SS morphants did not show a significant difference ($P = 0.1608$) between each other in head to length ratio. (**F**) Maximum intensity projections of confocal images showing FM1–43 dye uptake in neuromast cells of 9ng ATG and SS morpholino injected larvae vs 9ng control injected larvae at 5 dpf. The right panels show that neuromast cells of *stx4*-morpholino injected larvae do not uptake FM1–43 dye as compared to 9ng control injected in the left panel. Scale bar: 20μm. All data shown are mean ± SD with two-tailed unpaired Student's *t*-test.

detailed expression in hair cells and surrounding cells over four developmental stages [E16, postnatal day (P)0, P4 and P7] in the cochleae and utricles of mice obtained via RNA sequencing (58). These data were supplemented with a microarray dataset containing expression data over six developmental stages: E12, E13, E16, P0, P6 and P15 in spiral ganglion neurons and vestibular ganglion neurons (59).

Last, the gene Expression Analysis Resource (gEAR) was used to visualize *Stx4a* expression in single cells of the cochlear epithelium during mouse development (60). Single-cell RNA sequencing data of the sensory epithelium of CD1 mouse embryos at E14, E16, P1 and P7 were interrogated and plotted using gEAR's analysis suite (61). *Stx4a* expression was grouped based on cell groups in four overarching classes: developing supporting cells, developing prosensory cells, developing sensory cells and developing greater epithelial ridge cells, each of which were further divided into subclasses (61).

Whole mount immunostaining of STX4A in mouse inner ears

All the animal work was approved by the University of Maryland, Baltimore Institutional Animal Care and use Committee (IACUC 420002). Inner ears were dissected from P12 mice and fixed in 4% paraformaldehyde (PFA) in phosphate buffered saline (PBS) overnight. After fixation temporal bones were decalcified in 0.25 M EDTA solution overnight. For whole mount immunostaining, the cochleae were micro-dissected and were subjected to blocking for 1 h with 10% normal goat serum in PBS containing 0.25% tritonX100, followed by overnight incubation at 4°C with primary antibody (1:200) in 3% normal goat serum with PBS. Primary antibodies used are rabbit anti syntaxin 4 (Synaptic systems 110042) and mouse anti CTBP2 (Thermo Fisher MA5-26926). F-Actin was stained using phalloidin 647nm (1:300), and nuclei were stained with 4′,6-diamidino-2-phenylindole (DAPI). Confocal images were acquired from Nikon Spinning disk W1 confocal microscope, and images were processed using ImageJ software.

Zebrafish morpholino-based knockdown of *stx4*

WT AB/Tübingen (AB/TU) zebrafish were used for breeding. The embryos attained were injected between the 1- and 2-cell stage with 3ng, 6ng, 9ng and 12ng to check dosage response of either an *stx4* based ATG start codon morpholino (5′-CGCATTTTCGATGTATTTTATGGCC-3′) or a SS morpholino (5′-AGCTAAATTACTTACTGTCCTCTGG-3′) (Fig. 3A). Approximately 9ng dosage was selected for further analysis to assess HI using ABER and FM1–43 uptake. A 9ng control morpholino (5′-CCTCTTACCTCAGTTACAATTTATA-3′) was also injected to observe the morphological defects and to assess the startle response differences (Fig. 3A, B and D). At 5 dpf, the startle response of 9ng ATG and SS morpholino injected zebrafish larvae along with 9ng injected controls were measured using Zebralab Viewpoint System. Following the protocol by Vona *et al.* (62) for a similar system, the experiment was carried out for 4 min. Twelve stimuli of 1kHz for 100 ms were given after every 20s. Sensitivity detection was set to 20, while the burst threshold was selected as 50 pixels and freeze was set as 10 pixels. The data for larva were excluded if spontaneous response was shown 2s before stimulus or if they showed random movements for more than six stimuli. The movement was calculated in milliseconds. However, we calculated the average response of each larva for 12 sound stimuli and plotted this in Figure 3B. A Student's *t*-test was used to determine if the differential activities between control and morphants were statistically significant. The larvae from both groups were then collected for imaging, RT-PCR and FM1–43 uptake. For FM1–43 dye update, larvae were exposed to the fixable version of the dye (Catalog #F35355) diluted to 3μM concentration in hanks' balanced salt solution (HBSS) for 15s and then fixed in 4% PFA. Nuclei were labelled with DAPI, and confocal images were acquired using Nikon W100 confocal microscope and images were processed in ImageJ (63).

Data Submission

The variant reported in this study was submitted to ClinVar (Accession number: SCV002499562).

Supplementary Material

Supplementary Material is available at *HMG* online.

Conflict of Interest statement. The authors declare no conflict of interest.

Funding

Higher Education Commission of Pakistan (to W.A.) and National Institutes of Health (NIH)-National Institute of Deafness and other Disorders (grants R01 DC011651 and R01 DC003594 to S.M.L.).

References

1. Smith, R.J.H., Bale, J.F. and White, K.R. (2005) Sensorineural hearing loss in children. *Lancet*, **365**, 879–890.
2. Egilmez, O.K. and Kalcioglu, M.T. (2016) Genetics of nonsyndromic congenital hearing loss. *Scientifica (Cairo)*, **2016**, 7576064.
3. Van Camp, G. and Smith, R.J. Hereditary hearing loss homepage. Hereditary hearing loss homepage. https://hereditaryhearingloss.org/ (accessed 8 March 2022).
4. Seligman, K.L., Shearer, A.E., Frees, K., Nishimura, C., Kolbe, D., Dunn, C., Hansen, M.R., Gantz, B.J. and Smith, R.J.H. (2021) Genetic causes of hearing loss in a large cohort of cochlear implant recipients. *Otolaryngol. Head Neck Surg.*, **166**, 734–737.
5. Zazo Seco, C., Wesdorp, M., Feenstra, I., Pfundt, R., Hehir-Kwa, J.Y., Lelieveld, S.H., Castelein, S., Gilissen, C., de Wijs, I.J., Admiraal, R.J. *et al.* (2017) The diagnostic yield of whole-exome sequencing targeting a gene panel for hearing impairment in The Netherlands. *Eur. J. Hum. Genet.*, **25**, 308–314.
6. Yuan, Y., Li, Q., Su, Y., Lin, Q., Gao, X., Liu, H., Huang, S., Kang, D., Todd, N.W., Mattox, D. *et al.* (2020) Comprehensive genetic testing of Chinese SNHL patients and variants interpretation using ACMG guidelines and ethnically matched normal controls. *Eur. J. Hum. Genet.*, **28**, 231–243.
7. Sloan-Heggen, C.M., Bierer, A.O., Shearer, A.E., Kolbe, D.L., Nishimura, C.J., Frees, K.L., Ephraim, S.S., Shibata, S.B., Booth, K.T., Campbell, C.A. *et al.* (2016) Comprehensive genetic testing in the clinical evaluation of 1119 patients with hearing loss. *Hum. Genet.*, **135**, 441–450.
8. Teng, F.Y., Wang, Y. and Tang, B.L. (2001) The syntaxins. *Genome Biol.*, **2**, REVIEWS3012.
9. Südhof, T.C. and Rothman, J.E. (2009) Membrane fusion: grappling with SNARE and SM proteins. *Science*, **323**, 474–477.
10. Safieddine, S., Ly, C.D., Wang, Y.-X., Wang, C.Y., Kachar, B., Petralia, R.S. and Wenthold, R.J. (2002) Ocsyn, a novel syntaxin-interacting protein enriched in the subapical region of inner hair cells. *Mol. Cell. Neurosci.*, **20**, 343–353.

11. Safieddine, S. and Wenthold, R.J. (1999) SNARE complex at the ribbon synapses of cochlear hair cells: analysis of synaptic vesicle- and synaptic membrane-associated proteins. *Eur. J. Neurosci.*, **11**, 803–812.
12. Jian, X., Boerwinkle, E. and Liu, X. (2014) In silico prediction of splice-altering single nucleotide variants in the human genome. *Nucleic Acids Res.*, **42**, 13534–13544.
13. Reese, M.G., Eeckman, F.H., Kulp, D. and Haussler, D. (1997) Improved splice site detection in Genie. *J. Comput. Biol.*, **4**, 311–323.
14. Desmet, F.-O., Hamroun, D., Lalande, M., Collod-Béroud, G., Claustres, M. and Béroud, C. (2009) Human Splicing Finder: an online bioinformatics tool to predict splicing signals. *Nucleic Acids Res.*, **37**, e67.
15. Kowalski, M.H., Qian, H., Hou, Z., Rosen, J.D., Tapia, A.L., Shan, Y., Jain, D., Argos, M., Arnett, D.K., Avery, C. *et al.* (2019) Use of >100,000 NHLBI Trans-Omics for Precision Medicine (TOPMed) Consortium whole genome sequences improves imputation quality and detection of rare variant associations in admixed African and Hispanic/Latino populations. *PLoS Genet.*, **15**, e1008500.
16. Karczewski, K.J., Francioli, L.C., Tiao, G., Cummings, B.B., Alföldi, J., Wang, Q., Collins, R.L., Laricchia, K.M., Ganna, A., Birnbaum, D.P. *et al.* (2020) The mutational constraint spectrum quantified from variation in 141,456 humans. *Nature*, **581**, 434–443.
17. Scott, E.M., Halees, A., Itan, Y., Spencer, E.G., He, Y., Azab, M.A., Gabriel, S.B., Belkadi, A., Boisson, B., Abel, L. *et al.* (2016) Characterization of Greater Middle Eastern genetic variation for enhanced disease gene discovery. *Nat. Genet.*, **48**, 1071–1076.
18. Lyles, C.R., Lunn, M.R., Obedin-Maliver, J. and Bibbins-Domingo, K. (2018) The new era of precision population health: insights for the All of Us Research Program and beyond. *J. Transl. Med.*, **16**, 211.
19. GTEx Consortium (2013) The Genotype-Tissue Expression (GTEx) project. *Nat. Genet.*, **45**, 580–585.
20. Schrauwen, I., Hasin-Brumshtein, Y., Corneveaux, J.J., Ohmen, J., White, C., Allen, A.N., Lusis, A.J., Van Camp, G., Huentelman, M.J. and Friedman, R.A. (2016) A comprehensive catalogue of the coding and non-coding transcripts of the human inner ear. *Hear. Res.*, **333**, 266–274.
21. Khajavi, M., Inoue, K. and Lupski, J.R. (2006) Nonsense-mediated mRNA decay modulates clinical outcome of genetic disease. *Eur. J. Hum. Genet.*, **14**, 1074–1081.
22. Min, J., Okada, S., Kanzaki, M., Elmendorf, J.S., Coker, K.J., Ceresa, B.P., Syu, L.J., Noda, Y., Saltiel, A.R. and Pessin, J.E. (1999) Synip: a novel insulin-regulated syntaxin 4-binding protein mediating GLUT4 translocation in adipocytes. *Mol. Cell*, **3**, 751–760.
23. Foley, K., Boguslavsky, S. and Klip, A. (2011) Endocytosis, recycling, and regulated exocytosis of glucose transporter 4. *Biochemistry*, **50**, 3048–3061.
24. Kennedy, M.J., Davison, I.G., Robinson, C.G. and Ehlers, M.D. (2010) Syntaxin-4 defines a domain for activity-dependent exocytosis in dendritic spines. *Cell*, **141**, 524–535.
25. Kennedy, M.J. and Ehlers, M.D. (2011) Mechanisms and function of dendritic exocytosis. *Neuron*, **69**, 856–875.
26. Bennett, M.K., Garcia-Arrarás, J.E., Elferink, L.A., Peterson, K., Fleming, A.M., Hazuka, C.D. and Scheller, R.H. (1993) The syntaxin family of vesicular transport receptors. *Cell*, **74**, 863–873.
27. Yang, C., Coker, K.J., Kim, J.K., Mora, S., Thurmond, D.C., Davis, A.C., Yang, B., Williamson, R.A., Shulman, G.I. and Pessin, J.E. (2001) Syntaxin 4 heterozygous knockout mice develop muscle insulin resistance. *J. Clin. Invest.*, **107**, 1311–1318.
28. Oh, E., Ahn, M., Afelik, S., Becker, T.C., Roep, B.O. and Thurmond, D.C. (2018) Syntaxin 4 expression in pancreatic β-cells promotes islet function and protects functional β-cell mass. *Diabetes*, **67**, 2626–2639.
29. Paumet, F., Le Mao, J., Martin, S., Galli, T., David, B., Blank, U. and Roa, M. (2000) Soluble NSF attachment protein receptors (SNAREs) in RBL-2H3 mast cells: functional role of syntaxin 4 in exocytosis and identification of a vesicle-associated membrane protein 8-containing secretory compartment. *J. Immunol.*, **164**, 5850–5857.
30. Saito, T., Okada, S., Yamada, E., Ohshima, K., Shimizu, H., Shimomura, K., Sato, M., Pessin, J.E. and Mori, M. (2003) Syntaxin 4 and Synip (syntaxin 4 interacting protein) regulate insulin secretion in the pancreatic beta HC-9 cell. *J. Biol. Chem.*, **278**, 36718–36725.
31. Volchuk, A., Wang, Q., Ewart, H.S., Liu, Z., He, L., Bennett, M.K. and Klip, A. (1996) Syntaxin 4 in 3T3-L1 adipocytes: regulation by insulin and participation in insulin-dependent glucose transport. *Mol. Biol. Cell*, **7**, 1075–1082.
32. Mollinedo, F., Calafat, J., Janssen, H., Martín-Martín, B., Canchado, J., Nabokina, S.M. and Gajate, C. (2006) Combinatorial SNARE complexes modulate the secretion of cytoplasmic granules in human neutrophils. *J. Immunol.*, **177**, 2831–2841.
33. Olson, A.L., Knight, J.B. and Pessin, J.E. (1997) Syntaxin 4, VAMP2, and/or VAMP3/cellubrevin are functional target membrane and vesicle SNAP receptors for insulin-stimulated GLUT4 translocation in adipocytes. *Mol. Cell. Biol.*, **17**, 2425–2435.
34. Yang, S., Cai, Q., Vethanayagam, R.R., Wang, J., Yang, W. and Hu, B.H. (2016) Immune defense is the primary function associated with the differentially expressed genes in the cochlea following acoustic trauma. *Hear. Res.*, **333**, 283–294.
35. Meyers, J.R., MacDonald, R.B., Duggan, A., Lenzi, D., Standaert, D.G., Corwin, J.T. and Corey, D.P. (2003) Lighting up the senses: FM1-43 loading of sensory cells through nonselective ion channels. *J. Neurosci.*, **23**, 4054–4065.
36. Kachar, B., Battaglia, A. and Fex, J. (1997) Compartmentalized vesicular traffic around the hair cell cuticular plate. *Hear. Res.*, **107**, 102–112.
37. Kindt, K.S. and Sheets, L. (2018) Transmission disrupted: modeling auditory synaptopathy in zebrafish. *Front. Cell Dev. Biol.*, **6**, 114.
38. Roux, I., Safieddine, S., Nouvian, R., Grati, M., Simmler, M.-C., Bahloul, A., Perfettini, I., Gall, M.L., Rostaing, P., Hamard, G. *et al.* (2006) Otoferlin, defective in a human deafness form, is essential for exocytosis at the auditory ribbon synapse. *Cell*, **127**, 277–289.
39. Perl, E., Ravisankar, P., Beerens, M.E., Mulahasanovic, L., Smallwood, K., Sasso, M.B., Wenzel, C., Ryan, T.D., Komár, M., Bove, K.E. *et al.* (2022) Stx4 is required to regulate cardiomyocyte Ca2+ handling during vertebrate cardiac development. *HGG Adv.*, **3**, 100115.
40. Sambrook, J. and Russell, D.W. (2006) Purification of nucleic acids by extraction with phenol:chloroform. *CSH Protoc.*, **2006**, pdb.prot4455.
41. Schultz, J.M., Khan, S.N., Ahmed, Z.M., Riazuddin, S., Waryah, A.M., Chhatre, D., Starost, M.F., Ploplis, B., Buckley, S., Velásquez, D. *et al.* (2009) Noncoding mutations of HGF are associated with nonsyndromic hearing loss, DFNB39. *Am. J. Hum. Genet.*, **85**, 25–39.
42. Shahzad, M., Sivakumaran, T.A., Qaiser, T.A., Schultz, J.M., Hussain, Z., Flanagan, M., Bhinder, M.A., Kissell, D., Greinwald, J.H., Khan, S.N. *et al.* (2013) Genetic analysis through OtoSeq of Pakistani families segregating prelingual hearing loss. *Otolaryngol. Head Neck Surg.*, **149**, 478–487.

43. Riazuddin, S., Belyantseva, I.A., Giese, A.P.J., Lee, K., Indzhykulian, A.A., Nandamuri, S.P., Yousaf, R., Sinha, G.P., Lee, S., Terrell, D. *et al.* (2012) Alterations of the CIB2 calcium- and integrin-binding protein cause Usher syndrome type 1J and nonsyndromic deafness DFNB48. *Nat. Genet.*, **44**, 1265–1271.
44. Li, H. and Durbin, R. (2009) Fast and accurate short read alignment with Burrows-Wheeler transform. *Bioinformatics*, **25**, 1754–1760.
45. McKenna, A., Hanna, M., Banks, E., Sivachenko, A., Cibulskis, K., Kernytsky, A., Garimella, K., Altshuler, D., Gabriel, S., Daly, M. *et al.* (2010) The Genome Analysis Toolkit: a MapReduce framework for analyzing next-generation DNA sequencing data. *Genome Res.*, **20**, 1297–1303.
46. Yang, H. and Wang, K. (2015) Genomic variant annotation and prioritization with ANNOVAR and wANNOVAR. *Nat. Protoc.*, **10**, 1556–1566.
47. Liu, X., Wu, C., Li, C. and Boerwinkle, E. (2016) dbNSFP v3.0: a one-stop database of functional predictions and annotations for human nonsynonymous and splice-site SNVs. *Hum. Mutat.*, **37**, 235–241.
48. Rentzsch, P., Witten, D., Cooper, G.M., Shendure, J. and Kircher, M. (2019) CADD: predicting the deleteriousness of variants throughout the human genome. *Nucleic Acids Res.*, **47**, D886–D894.
49. Krumm, N., Sudmant, P.H., Ko, A., O'Roak, B.J., Malig, M., Coe, B.P., Quinlan, A.R., Nickerson, D.A. and Eichler, E.E. (2012) Copy number variation detection and genotyping from exome sequence data. *Genome Res.*, **22**, 1525–1532.
50. Geoffroy, V., Herenger, Y., Kress, A., Stoetzel, C., Piton, A., Dollfus, H. and Muller, J. (2018) AnnotSV: an integrated tool for structural variations annotation. *Bioinformatics*, **34**, 3572–3574.
51. Smedley, D., Haider, S., Ballester, B., Holland, R., London, D., Thorisson, G. and Kasprzyk, A. (2009) BioMart–biological queries made easy. *BMC Genomics*, **10**, 22.
52. MacDonald, J.R., Ziman, R., Yuen, R.K.C., Feuk, L. and Scherer, S.W. (2014) The Database of Genomic Variants: a curated collection of structural variation in the human genome. *Nucleic Acids Res.*, **42**, D986–D992.
53. Danecek, P., Bonfield, J.K., Liddle, J., Marshall, J., Ohan, V., Pollard, M.O., Whitwham, A., Keane, T., McCarthy, S.A., Davies, R.M. *et al.* (2021) Twelve years of SAMtools and BCFtools. *Gigascience*, **10**, giab008.
54. Seelow, D., Schuelke, M., Hildebrandt, F. and Nürnberg, P. (2009) HomozygosityMapper–an interactive approach to homozygosity mapping. *Nucleic Acids Res.*, **37**, W593–W599.
55. Silberstein, M., Tzemach, A., Dovgolevsky, N., Fishelson, M., Schuster, A. and Geiger, D. (2006) Online system for faster multipoint linkage analysis via parallel execution on thousands of personal computers. *Am. J. Hum. Genet.*, **78**, 922–935.
56. Brunskill, E.W., Potter, A.S., Distasio, A., Dexheimer, P., Plassard, A., Aronow, B.J. and Potter, S.S. (2014) A gene expression atlas of early craniofacial development. *Dev. Biol.*, **391**, 133–146.
57. Shen, J., Scheffer, D.I., Kwan, K.Y. and Corey, D.P. (2015) SHIELD: an integrative gene expression database for inner ear research. *Database (Oxford)*, **2015**, bav071.
58. Scheffer, D.I., Shen, J., Corey, D.P. and Chen, Z.-Y. (2015) Gene expression by mouse inner ear hair cells during development. *J. Neurosci.*, **35**, 6366–6380.
59. Lu, C.C., Appler, J.M., Houseman, E.A. and Goodrich, L.V. (2011) Developmental profiling of spiral ganglion neurons reveals insights into auditory circuit assembly. *J. Neurosci.*, **31**, 10903–10918.
60. Orvis, J., Gottfried, B., Kancherla, J., Adkins, R.S., Song, Y., Dror, A.A., Olley, D., Rose, K., Chrysostomou, E., Kelly, M.C. *et al.* (2021) gEAR: Gene Expression Analysis Resource portal for community-driven, multi-omic data exploration. *Nat. Methods*, **18**, 843–844.
61. Kolla, L., Kelly, M.C., Mann, Z.F., Anaya-Rocha, A., Ellis, K., Lemons, A., Palermo, A.T., So, K.S., Mays, J.C., Orvis, J. *et al.* (2020) Characterization of the development of the mouse cochlear epithelium at the single cell level. *Nat. Commun.*, **11**, 1–16.
62. Vona, B., Mazaheri, N., Lin, S.-J., Dunbar, L.A., Maroofian, R., Azaiez, H., Booth, K.T., Vitry, S., Rad, A., Rüschendorf, F. *et al.* (2021) A biallelic variant in CLRN2 causes non-syndromic hearing loss in humans. *Hum. Genet.*, **140**, 915–931.
63. Schneider, C.A., Rasband, W.S. and Eliceiri, K.W. (2012) NIH Image to ImageJ: 25 years of image analysis. *Nat. Methods*, **9**, 671–675.